

# The Sound of Silence: Ionic Mechanisms Encoding Sound Termination

Cornelia Kopp-Scheinflug,<sup>1</sup> Adam J.B. Tozer,<sup>1</sup> Susan W. Robinson,<sup>1</sup> Bruce L. Tempel,<sup>2</sup> Matthias H. Hennig,<sup>3,4</sup> and Ian D. Forsythe<sup>1,\*</sup>

<sup>1</sup>MRC Toxicology Unit, Hodgkin Building, University of Leicester, Leicester LE1 9HN, UK

<sup>2</sup>VM Bloedel Hearing Res. Ctr. and Department of Otolaryngology, University of Washington, Seattle, WA 98195, USA

<sup>3</sup>Institute for Adaptive and Neural Computation, School of Informatics, University of Edinburgh, EH8 9AB Edinburgh, UK

<sup>4</sup>Centre for Systems Biology at Edinburgh, CH Waddington Building, The Kings Buildings Campus, EH9 3JD Edinburgh, UK

\*Correspondence: [idf@le.ac.uk](mailto:idf@le.ac.uk)

DOI 10.1016/j.neuron.2011.06.028

## SUMMARY

Offset responses upon termination of a stimulus are crucial for perceptual grouping and gap detection. These gaps are key features of vocal communication, but an ionic mechanism capable of generating fast offsets from auditory stimuli has proven elusive. Offset firing arises in the brainstem superior paraolivary nucleus (SPN), which receives powerful inhibition during sound and converts this into precise action potential (AP) firing upon sound termination. Whole-cell patch recording *in vitro* showed that offset firing was triggered by IPSPs rather than EPSPs. We show that AP firing can emerge from inhibition through integration of large IPSPs, driven by an extremely negative chloride reversal potential ( $E_{Cl}$ ), combined with a large hyperpolarization-activated nonspecific cationic current ( $I_H$ ), with a secondary contribution from a T-type calcium conductance ( $I_{TCa}$ ). On activation by the IPSP,  $I_H$  potentially accelerates the membrane time constant, so when the sound ceases, a rapid repolarization triggers multiple offset APs that match onset timing accuracy.

## INTRODUCTION

The duration and termination of a sensory input are universal parameters underlying sensory processing that require some element of neural computation. This is especially true in the auditory system, where preservation of timing information is important for sound localization, auditory scene analysis, and communication (Snell and Frisina, 2000). The mammalian auditory brainstem possesses circuits involved in gap detection and sound duration encoding (Kadner and Berrebi, 2008; Kadner et al., 2006) in which the superior paraolivary nucleus (SPN) and the medial nucleus of the trapezoid body (MNTB; Banks and Smith, 1992; Kuwabara and Zook, 1991) are key components (Figure 1A).

The rodent SPN (referred to as SPON in rats: Saldaña and Berrebi, 2000) is considered to be the homolog of the dorsomedial paraolivary nucleus in other mammals (Grothe and Park, 2000).

The ubiquitous presence of this nucleus across many mammalian species, independent of their specialization for low- or high-frequency sound localization, also suggests that the SPN is involved in functions other than sound localization (Behrend et al., 2002; Dehmel et al., 2002; Kulesza, 2008; Kulesza et al., 2003; Schofield, 1995; Zook and Casseday, 1982). The SPN receives a weak bilateral (predominantly contralateral) excitatory input from the cochlear nuclei (Kuwabara et al., 1991) and a strong, tonotopically ordered inhibitory input from the MNTB (Banks and Smith, 1992; Sommer et al., 1993). During a sound, action potential (AP) firing is suppressed by MNTB inhibition, but when the sound ceases, the SPN is released from this inhibition and generates rebound APs as an “offset response” (Behrend et al., 2002; Dehmel et al., 2002; Kulesza et al., 2003). This IPSP-induced offset firing is mediated by glycine receptors (Kadner and Berrebi, 2008) and three mechanisms have been postulated to explain the offset firing:

- (1) Coincident excitation and inhibition suppress firing during the sound, but the excitation outlasts the inhibition (discussed in Kulesza et al., 2003).
- (2) An initial evoked IPSP becomes depolarizing as a consequence of an activity-dependent shift in  $E_{Cl}$  (Kaila et al., 1997).
- (3) The offset response is generated by the intrinsic conductances of the SPN neuron. It seems unlikely that release from MNTB inhibition could be the sole mechanism generating offset firing, since other major targets of MNTB inhibition (such as the medial and lateral superior olives) rarely exhibit offset firing (Barnes-Davies et al., 2004; Scott et al., 2005).

We demonstrate that offset firing is an intrinsic activity of SPN neurons with the ionic mechanism requiring three crucial elements: sound-evoked IPSPs, a large electrochemical chloride gradient, and the combination of a hyperpolarization-activated cation current,  $I_H$ , with a T-type calcium current,  $I_{TCa}$ . Modeling has suggested that  $I_H$  could contribute to stimulus duration encoding (Hooper et al., 2002); our results provide experimental evidence for this but also demonstrate the crucial importance of the IPSP and enhanced chloride gradients, so that the inhibition can provide sufficient hyperpolarization to activate  $I_H$  in response to physiological sensory input. We have confirmed this interpretation using sound-evoked SPN single-unit recordings

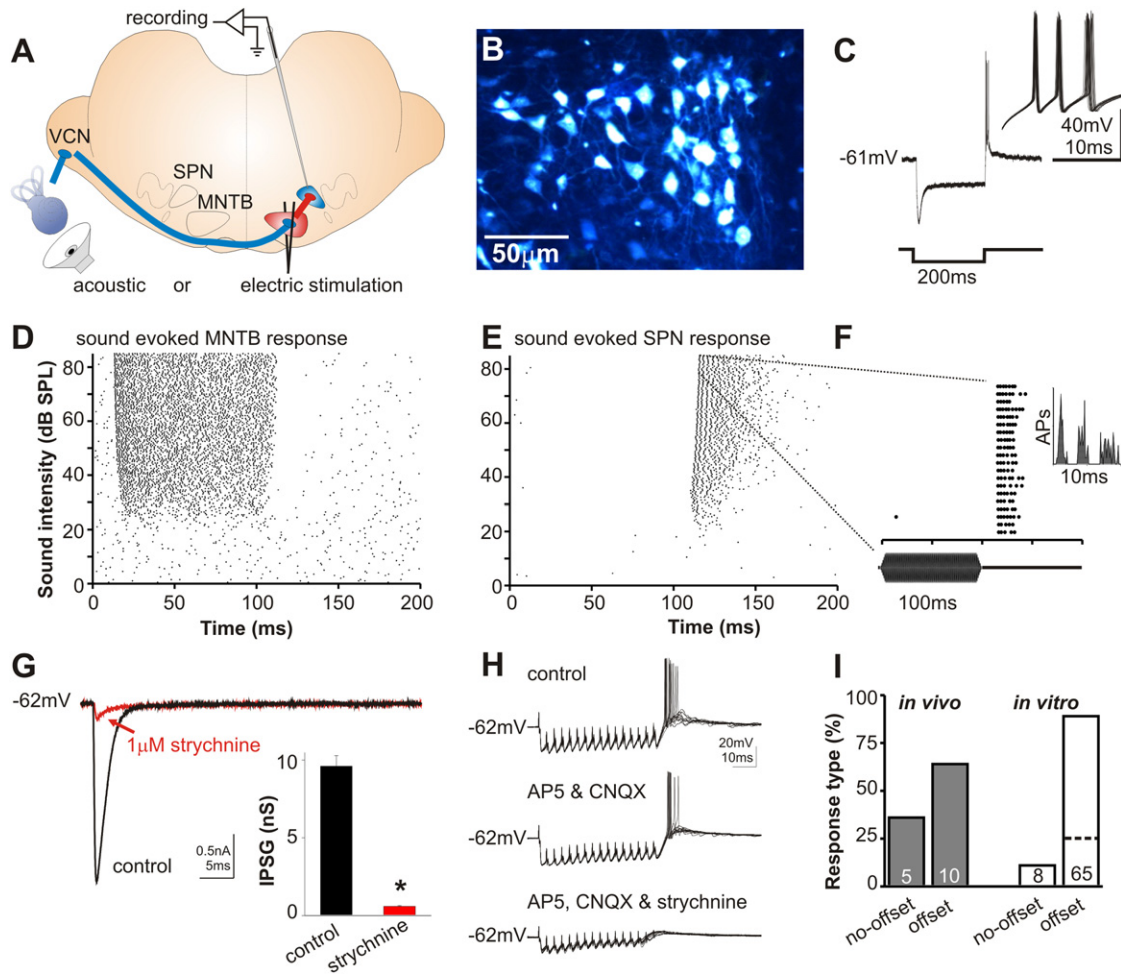


**Figure 1. The MNTB Provides Sufficient Inhibition to Cause Offset Responses in the Mouse SPN In Vivo and In Vitro**

(A) Diagram of the brainstem at the level of the superior olivary complex showing the stimulation and recording sites.  
 (B) Retrograde labeling of SPN cells after fluorogold injection into the ipsilateral IC.  
 (C) SPN in vitro: whole-cell patch recording under current clamp (upper trace) showing the typical hyperpolarization and “sag” during a 200 ms hyperpolarizing current step (–400 pA, lower trace). After the end of the current step the potential rapidly returns to rest with a burst of APs. Inset: ten superimposed traces at higher gain shows that the rhythmic offset burst usually contains two to four well-timed APs.  
 (D) MNTB in vivo: dot raster plot to a repetitive (10 runs/100 ms stimulus) sound stimulation at CF (17.8 kHz) with intensity increasing from 0 to 80 dB SPL. Firing increases with intensity and spontaneous firing is suppressed afterwards.  
 (E) SPN in vivo: dot raster plot for a repetitive (10 runs/100 ms stimulus) sound stimulation at CF (15.4 kHz) with intensity increasing from 0 to 80 dB SPL. Spontaneous activity is suppressed during sound stimulation while offset firing increases with sound intensity.  
 (F) SPN single-unit recording in vivo during 100 ms tone stimulation (lower trace) at CF/80 dB SPL. The dot-raster plot shows a well-timed offset response. Inset: the PSTH has distinct multiple peaks, indicating rhythmicity of the offset response.  
 (G) SPN in vitro: IPSCs evoked by electrical stimulation of the MNTB are blocked by strychnine (1  $\mu$ M).  
 (H) SPN in vitro: synaptic stimulation (of MNTB) at 100 Hz/100 ms produced a reliable offset response with or without contributions from excitatory synapses (upper and middle trace, respectively). Additional application of strychnine (lower trace) caused the IPSP hyperpolarization to decline and the offset response was eliminated.  
 (I) The proportion of SPN cells with and without offset firing in vivo and in vitro. The dotted line in the in vitro offset-bar (far right) represents the subpopulation of cells with only one AP in the offset response.

in vivo, characterized the conductances using voltage clamp in vitro, and demonstrated that these conductances are sufficient to explain the results by computational modeling. The result is a physiologically elegant solution to computation of sound termination: a cell-specific conversion of inhibition into excitatory AP firing, which enhances timing accuracy and provides crucial information for downstream duration encoding.

## RESULTS

### SPN Neurons Show Burst Offset Firing In Vitro and In Vivo

The majority of SPN neurons showed AP firing as an offset response following sound stimulation in vivo (64%, extracellular single unit,  $n = 15$ , Figures 1E, 1F, and 1I) or following

hyperpolarization in vitro (89%, whole-cell patch clamp,  $n = 70$ , Figures 1C, 1H, and 1I). A minority of neurons showed no offset firing upon hyperpolarization (Figure 1I), but instead showed sustained or onset firing in vivo, as seen in other species (Behrend et al., 2002; Dehmel et al., 2002). The offset firing characteristically exhibited an intrinsic rhythm observed as multiple distinct peaks in the poststimulus time histogram (PSTH; Figure 1F, inset). The average number of APs in the offset response was  $3.5 \pm 0.4$  ( $n = 65$ ) with an interspike interval of  $1.85 \text{ ms} \pm 0.19 \text{ ms}$  ( $n = 26$  cells) between the first two APs and increasing variability for the subsequent APs, as shown in the inset in Figure 1C. A subpopulation of cells (25%; Figure 1I, dotted line) fired only one offset AP; these neurons lacked the very negative  $E_{Cl}$  (see below) and possessed an  $I_A$  type potassium current, suggesting that their role may differ. The differences were minor and we did not exclude these cells from the data set to avoid sample bias.

The offset firing pattern will be conserved on projection from the SPN to target neurons, and confirmation of a projection to the inferior colliculus (IC) in mice was obtained by retrograde labeling of SPN neurons after fluorogold injection into the IC (Figure 1B). The ionic mechanisms underlying this offset firing were investigated by studying the conductances activated around resting membrane potentials (RMP:  $-59.9 \pm 0.9 \text{ mV}$ ;  $n = 82$ ). A general characterization of the SPN neurons under voltage clamp in vitro showed that they possessed large sustained outward potassium currents in response to depolarization, including tetraethyl ammonium-sensitive Kv3 high voltage-activated currents and low voltage-activated, dendrotoxin-I sensitive Kv1 currents. Under current clamp SPN neurons had rapid time-course overshooting APs (absolute amplitude:  $12.1 \pm 1.5 \text{ mV}$ ; half-width:  $0.36 \pm 0.02 \text{ ms}$ ,  $n = 72$ , see also Figure S1, available online).

#### SPN Offset Firing Is Evoked by Glycinergic Input after MNTB Stimulation In Vivo and In Vitro

Sound-evoked firing in neurons of the MNTB and SPN show a reciprocal relationship. Presentation of a contralateral pure-tone stimulus at the characteristic frequency (CF) for an MNTB neuron gives continuous high-frequency AP firing for the duration of the stimulation, but firing is suppressed below spontaneous activity after the end of the sound (Figure 1D). MNTB AP firing exceeds spontaneous levels as sound intensity (0 to 80 dB SPL) passes threshold and monotonically increases until reaching a plateau firing rate (Figure 1D). The opposite occurs in the SPN; sound stimulation suppresses all firing during the sound but triggers offset firing after cessation of the sound (Figure 1E) with the number of APs continuously increasing with sound intensity (beyond threshold). Stimulation of the MNTB activated endogenous inhibition in SPN neurons in vitro, followed by offset APs (100 Hz train for 100 ms, Figure 1H, upper trace, see also Figure S2). Thus, acoustic stimulation, hyperpolarizing current injection, and electrically evoked IPSPs all resulted in similar offset firing. These results confirm the uniformity of evoked offset firing in both in vivo and in vitro recordings and support the use of in vitro methods to identify the ionic basis of SPN offset firing. IPSCs triggered by MNTB stimulation are blocked by the glycine receptor antagonist strychnine (1  $\mu\text{M}$ ), confirming the origin and transmitter of this inhibitory synaptic

projection (Figure 1G). In vivo recordings confirm that evoked glycinergic IPSPs trigger offset firing but do not exclude the possibility that EPSPs might also be involved. To test this hypothesis we used repetitive IPSPs evoked by electrical stimulation of the MNTB in vitro in the presence of AMPAR and NMDAR antagonists (50  $\mu\text{M}$  AP5, 10  $\mu\text{M}$  CNQX). Under these conditions, well-timed offset APs were generated (Figure 1H, middle trace) as the membrane potential rapidly depolarized back to resting levels at the end of the train, thus confirming that excitatory synaptic transmission was not necessary for offset firing. However, additional blockade of the glycinergic IPSCs diminished all offset firing in the SPN, identifying glycinergic inhibition as a major component of offset firing (Figure 1H, lower trace). Note that the IPSPs remain hyperpolarizing throughout the train of stimuli, including at the end of the stimulus, so the synaptic responses are not causing the depolarizing offset response. The obvious candidate for such a depolarizing offset response is the hyperpolarization-activated nonspecific cation conductance,  $I_H$ .

#### Large and Fast $I_H$ Currents Are Present and Generate Offset AP Firing

Current injection into SPN neurons (under current-clamp conditions) generated hyperpolarization that clearly exhibited the characteristic slow sag of the membrane potential over a period of around 50 ms, indicative of  $I_H$  activation (Figure 1C). Under voltage clamp, hyperpolarizing voltage steps from  $-61 \text{ mV}$  (Figure 2A) evoked an inward current with two components: first, a small instantaneous, ZD7288-insensitive leak current ( $I_l$ ) that exhibited some inward rectification (Figures 2A and 2B) and a mean conductance of  $32.8 \pm 2.9 \text{ nS}$  ( $n = 40$ ;  $E_K = -90 \text{ mV}$ ). Second, a more slowly activating and noninactivating inward current ( $I_H$ ) was observed. The magnitude of  $I_H$  was measured by subtraction of the instantaneous current ( $I_l$ ) from the sustained current ( $I_S$ ), giving a peak conductance of  $19.8 \pm 1.3 \text{ nS}$  ( $n = 40$ ;  $E_H = -40 \text{ mV}$ ; Figure 2B). The  $I_H$  current was inhibited by application of 20  $\mu\text{M}$  ZD7288 ( $n = 6$ ;  $p \leq 0.001$ ; Figure 2B). The voltage dependence of  $I_H$  activation was estimated from the tail currents ( $I_T$ , inset in Figure 2A), to which a Boltzmann function fit gave a half-maximum activation of  $-88.2 \pm 0.9 \text{ mV}$  with a slope of  $7.5 \pm 0.4 \text{ mV}$  ( $n = 30$ ; Figure 2C).  $I_H$  activation rate was measured on stepping to  $-130 \text{ mV}$  ( $n = 30$ ) and fit to the sum of two exponentials with respective time constants of:  $\tau_{\text{fast}}: 26.8 \pm 1.9 \text{ ms}$  and  $\tau_{\text{slow}}: 180.6 \pm 16.9 \text{ ms}$  (Figure 2D) of which the fast component contributed 70.6%. The activation rates slowed at more positive voltages ( $\tau_{\text{fast}} = 108.4 \pm 6.1 \text{ ms}$  at  $-70 \text{ mV}$ ,  $n = 30$ ) with an e-fold acceleration for 25 mV hyperpolarization. We postulated that the fast time course of  $I_H$  was due to the expression of HCN1 subunits (Nolan et al., 2004). Recordings from HCN1 knockout mice (KO) showed that the peak  $I_H$  current was indeed reduced to half that of the wild-type (WT; Figures 2A and 2B). The remaining  $I_H$  current in the HCN1-KO activated at more negative voltages and with a much slower time-course, consistent with mediation by HCN2 subunits (Figures 2A, 2C, and 2D).

Immunolabeling confirmed expression of HCN1 and HCN2 subunits in the SPN; HCN1 was predominantly associated with the somatic plasma membrane while HCN2 was largely

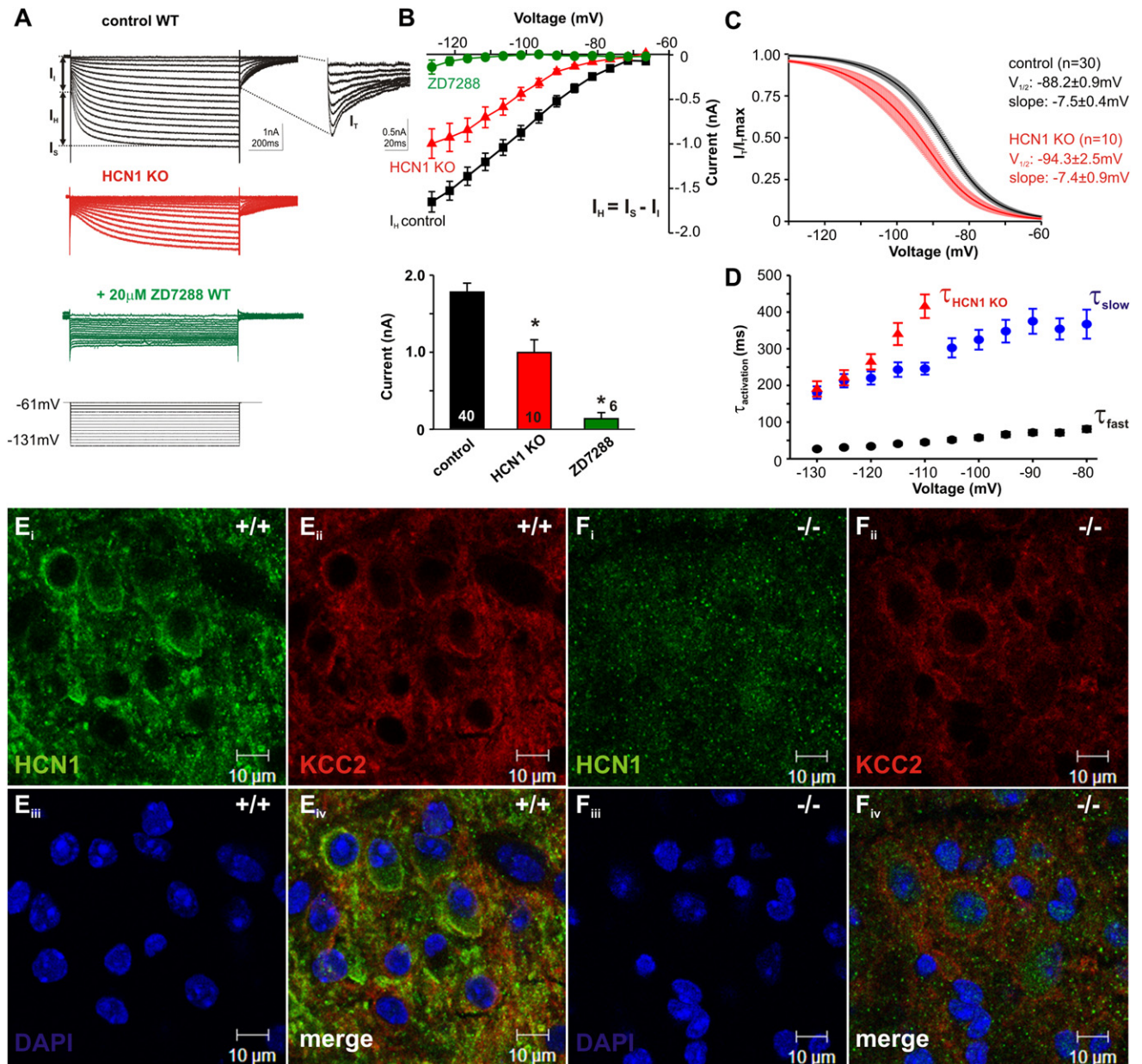


**Figure 2. SPN  $I_H$  Currents Are Large, Fast Activating, and Dominated by HCN1**

(A) WT:  $I_H$  currents evoked by step commands from a holding potential of  $-60$  mV to  $-130$  mV (voltage protocol plotted below) with the inset showing the  $I_H$  tail currents ( $I_T$ ). HCN1-KO:  $I_H$  currents evoked over the same voltage range are slow activating and low magnitude (red traces). Block of WT  $I_H$  currents by perfusion of  $20 \mu\text{M}$  ZD7288 revealed an instantaneous inward current (green traces).

(B) The difference between the sustained current ( $I_s$ ) and the instantaneous leak current ( $I_l$ ) indicates the  $I_H$  current in WT controls (black squares;  $n = 40$ ), in HCN1-KO (red triangles,  $n = 10$ ), and in WT after blockade by ZD7288 with some inward rectification (green circles,  $n = 6$ ). Bar graph shows mean current measured at  $-130$  mV for WT (black), HCN1-KO (red), and WT following ZD7288 ( $20 \mu\text{M}$ , green) application.

(C) The mean activation curve was plotted from tail currents of individual cells ( $I_T$ ; see inset in A) fitted to a Boltzmann equation (see methods) for WT controls (black,  $n = 30$ ) and HCN1-KO (red,  $n = 10$ ). The shaded areas show the range of the fit from individual cells.

(D) Activation kinetics of WT  $I_H$  were voltage dependent, and fit by a double exponential function dominated by the fast component:  $t_{\text{fast}}$  (black) and  $t_{\text{slow}}$  (blue).  $n = 30$ . Activation in the HCN1-KO (red) was much slower and was well fit by a single exponential function with similar values to the slow time constant of the WT data. Data are mean  $\pm$  SEM,  $n = 10$ .

(E and F) Immunohistochemical localization from SPN in WT (+/+) and the HCN1-KO (-/-), respectively: HCN1 (green, i), KCC2 (red, ii), DAPI (blue, iii), and combined (iv). Scale bars are as indicated.

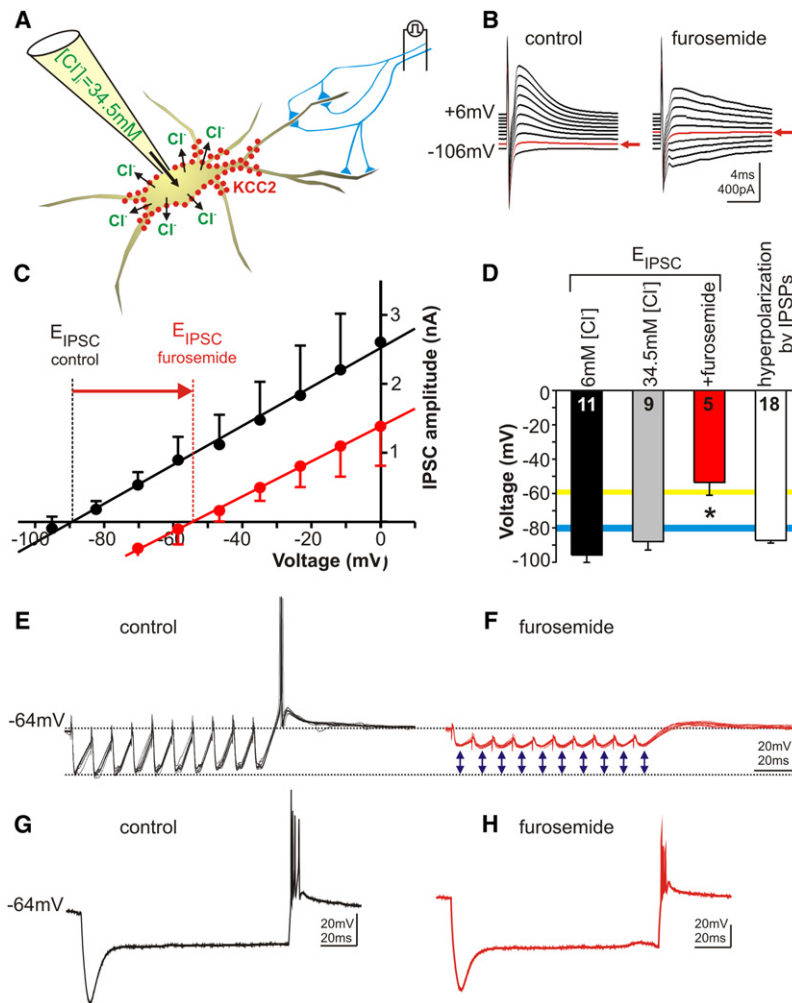


**Figure 3. The Outwardly Directed Chloride Transporter, KCC2, Maintains Low Intracellular Chloride and Increases IPSP Hyperpolarization**

(A) Diagram illustrating the experimental configuration: whole-cell patch solution contains 34.5 mM  $[Cl^-]_i$  giving a predicted  $E_{Cl^-}$  of  $-36$  mV, but the measured  $E_{IPSC}$  is  $-88$  mV, consistent with the hypothesis that somatic and proximal-dendritic KCC2 extrudes chloride entering the cell from the patch pipette.

(B) Superimposed IPSCs evoked by stimulation of the MNTB over a range of HPs ( $-106$  mV to  $+6$  mV) show the zero current potential (reversal potential, red arrow) under control (left) and during application of 0.5 mM furosemide (right).

(C) The mean I/V relationship for the IPSCs under control conditions (black) gave a reversal potential of  $-96$  mV. The I/V was repeated as furosemide (0.5 mM) washed onto the preparation and the reversal potential shifted to the right:  $-53$  mV (red).

(D) Plot of the relationship between  $E_{IPSC}$  and the membrane potential at which offset APs are first triggered under current clamp. Each bar is mean  $\pm$  SEM, with  $n$  indicated in the respective bar. The blue horizontal bar represents the average threshold for offset-AP generation ( $n = 82$ ). The yellow horizontal bar indicates the average resting membrane potential of SPN cells ( $n = 82$ ). When the patch solution contained 6 mM  $[Cl^-]$ , the  $E_{IPSC}$  was only a little more hyperpolarized from when it contains 34.5 mM  $[Cl^-]$ , because of the transporter. IPSCs under both conditions generate offset APs. But when furosemide is applied, the IPSC declines in amplitude as  $E_{IPSC}$  becomes less negative and now the IPSP can no longer evoke rebound APs. To underline the physiological relevance the white bar (right) shows the range of hyperpolarization induced by IPSPs. The fact that  $E_{IPSC}$  exceeds the voltage threshold for AP generation confirms that there is sufficient driving force for the IPSPs to trigger offset APs.

(E) MNTB stimulation at 100 Hz for 100 ms evoked large IPSPs, which generate offset AP firing in control SPN neurons.

(F) Application of furosemide (0.5 mM) reduced IPSP amplitudes (blue arrows) until no offset APs are triggered.

(G and H) Direct hyperpolarizing current injection evoked offset AP firing in the presence of furosemide.

expressed in the dendrites (Figures 2E and 2F; see also Figure S3). HCN3 and HCN4 were expressed at much lower levels or were absent from SPN cell bodies, but HCN4 staining was observed in trapezoid body axons (not shown). The presence of this large  $I_H$  conductance with a half-activation around  $-88$  mV suggests that the role of incoming glycinergic IPSPs could be to activate this conductance. But this raises two important physiological questions: (1) is the IPSP capable of sufficient hyperpolarization to activate  $I_H$ , and so in turn to generate an offset response? (2) Are any other conductances involved in offset firing?

#### Large IPSPs and Negative $E_{Cl^-}$ Are Maintained by KCC2, an Outward Chloride Transporter

The answer to the first question is that IPSPs are capable of triggering offset firing. However, in many neurons IPSPs are rather small because  $E_{Cl^-}$  may be less negative than  $E_K$  or, as in the immature brainstem, may be positive to the resting membrane potential. Experimental evidence supports the idea

that SPN neurons have a powerful outwardly directed chloride transporter and therefore large IPSPs. First, in an elegant study that employed gramicidin-perforated patch recording, the endogenous  $E_{Cl^-}$  in rat SPON neurons was shown to be around  $-100$  mV and this was associated with high membrane immunolabeling of the  $K^+Cl^-$  cotransporter, KCC2 (Löhrlke et al., 2005). In the current study  $E_{IPSC}$  was around  $-96 \pm 4.2$  mV ( $n = 11$ ) when a low chloride concentration (6 mM) was chosen for the patch pipette (Figure 3D). We tested the idea for an outwardly directed chloride pump, by setting an artificially high  $E_{Cl^-}$  and observing the change in  $E_{IPSP}$  while perfusing the chloride transporter antagonist, furosemide. A high chloride pipette solution (34.5 mM) gave a predicted  $E_{Cl^-}$  of  $-36$  mV, but  $E_{IPSC}$  remained negative at  $-88 \pm 4.8$  mV ( $n = 9$ , Figure 3D). Perfusion of furosemide (0.5 mM) caused a gradual shift in  $E_{IPSC}$  toward the  $E_{Cl^-}$  (Figures 3B and 3C) predicted by the Nernst equation. We conclude that mouse SPN neurons also possess the powerful outwardly directed chloride transporter KCC2 (Figure 2Gii), and that this maintains  $E_{Cl^-}$  at very negative levels.

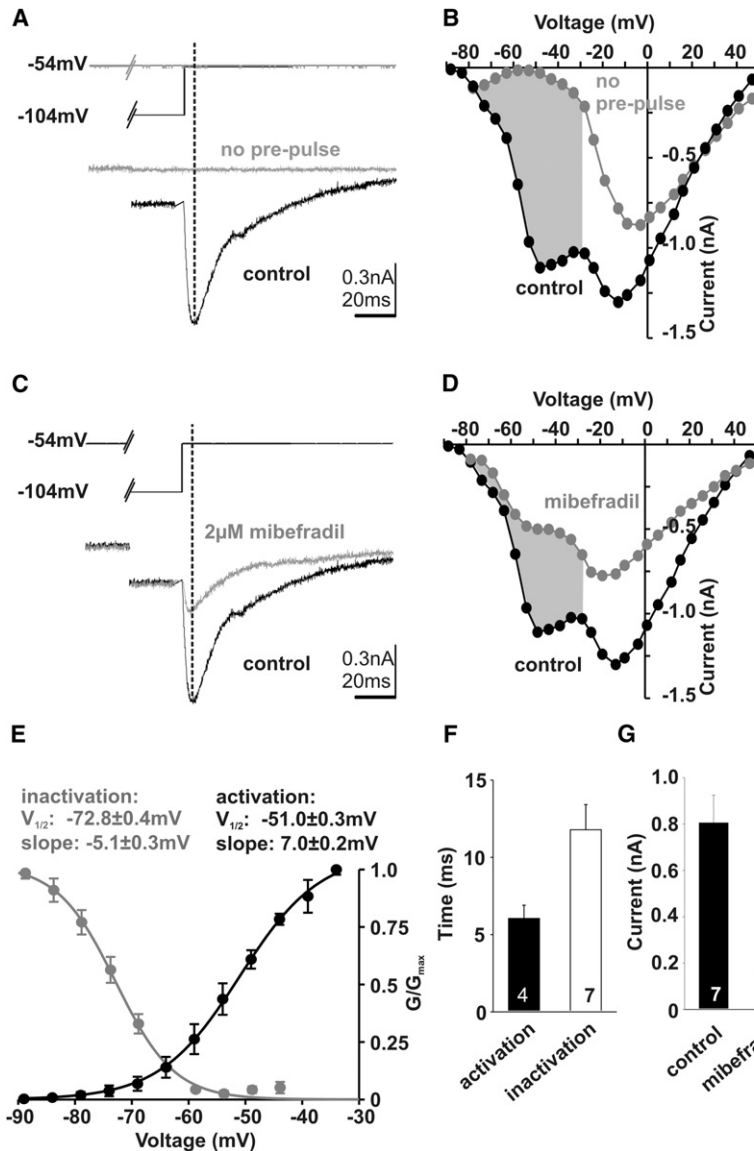


**Figure 4. A Low-Voltage-Activated T-Type Calcium Current ( $I_{TCa}$ ) Is Present in the SPN**

(A) An  $I_{TCa}$  current is evoked by a step command to  $-54\text{mV}$  when preceded by a prepulse to  $-104\text{mV}$  to remove inactivation (black trace). No  $I_{TCa}$  current was evoked without the prepulse (gray trace). Voltage-gated  $\text{Na}^+$  and  $\text{K}^+$  channels are blocked (see [Experimental Procedures](#)). (B) I/V relationship for SPN calcium currents evoked with the prepulse (black) showed low- and high-voltage-activated (HVA) subtypes; without a prepulse (gray) only HVA  $\text{Ca}^{2+}$  currents are generated. The voltage range dominated by  $I_{TCa}$  is shaded in gray. (C)  $I_{TCa}$  currents were inhibited by mibefradil ( $2\ \mu\text{M}$ , gray trace). (D) The I/V versus before (black) and after (gray) application of mibefradil with the block of  $I_{TCa}$  shaded in gray. (E) Activation/inactivation curves normalized to the maximal conductance for  $I_{TCa}$ . (F) Mean  $I_{TCa}$  time to peak (activation) and time to half-decay (inactivation) measured upon stepping to  $-54\text{mV}$  from a  $-104\text{mV}$  prepulse. (G) Average block of  $I_{TCa}$  currents by  $2\ \mu\text{M}$  mibefradil. The numbers,  $n$ , are indicated in each bar graph.

If this is true then physiological offset firing in response to synaptic input should also be blocked/suppressed by furosemide. Furosemide indeed caused the IPSPs to decline in amplitude and now the inhibitory input was insufficient to hyperpolarize the membrane to rebound-firing threshold ( $-81.13 \pm 1.3\text{mV}$ ,  $n = 71$ ; blue shaded area in [Figure 3D](#)) and so failed to trigger offset APs ([Figures 3E](#) and [3F](#)). As expected, direct hyperpolarizing current injections could still trigger offset APs after furosemide application ([Figures 3G](#) and [3H](#)). The control  $E_{IPSC}$  is sufficiently negative for the IPSPs to activate  $I_H$  and trigger offset APs. Furosemide ( $0.5\ \text{mM}$ ) did not block either  $I_H$  currents or glycinergic IPSCs directly ([Figure S4](#)).

**A Low-Voltage-Activated T-Type Calcium Current ( $I_{TCa}$ ) Also Contributes to Offset Firing**

In addition to  $I_H$ , the IPSP, and  $E_{Cl}$ , contributions from other conductances were implied because the current-voltage rela-

tionship showed a region of negative slope conductance at around  $-50$  to  $-30\text{mV}$ , suggesting large voltage-gated calcium currents in the SPN (see also [Figure S1F](#)). To measure calcium currents we used a  $\text{Cs}^+$  based patch solution that blocked the majority of  $\text{K}^+$  currents and combined this with use of appropriate voltage protocols and pharmacology under voltage clamp. From a holding potential of  $-54\text{mV}$ , and with no prior hyperpolarization, only high-voltage-activated (HVA)  $\text{Ca}^{2+}$  currents were observed on depolarization positive to  $-50\text{mV}$  ([Figure 4B](#), gray curve); however, a conditioning hyperpolarization to  $-104\text{mV}$  for  $400\ \text{ms}$  maximally activated a transient low-voltage-activated (LVA,  $I_{TCa}$ )  $\text{Ca}^{2+}$  current on stepping to  $-54\text{mV}$  ([Figure 4A](#)). The I/V relationship now showed two distinct components: a LVA  $\text{Ca}^{2+}$  current that peaked at around  $-50\text{mV}$ , and a HVA current that peaked at around  $-10\text{mV}$  ([Figure 4B](#), black curve).  $I_{TCa}$  currents were half-activated at  $-51.0 \pm 0.3\text{mV}$  ([Figure 4E](#)), were half-inactivated at  $-72.8 \pm 0.4\text{mV}$ , and had a conductance of  $20.1 \pm 2.9\ \text{nS}$  (at  $-54\text{mV}$ ;  $n = 7$ ;  $E_{Ca} = +50\text{mV}$ ). The activation kinetics of  $I_{TCa}$  upon stepping to  $-54\text{mV}$  were fast (time to peak:  $5.7 \pm 0.7\ \text{ms}$ ;  $n = 7$ ; [Figure 4F](#)). Inactivation was also fast, decaying with a single exponential ( $11.5 \pm 1.4\ \text{ms}$ ;  $n = 7$ ; at  $-54\text{mV}$ ; [Figure 4F](#)). Application of the  $I_{TCa}$  antagonist mibefradil ( $2\ \mu\text{M}$ , [Figures 4C](#), [4D](#), and [4G](#)) blocked 79% of the transient calcium current (measured on stepping to  $-54\text{mV}$ ;  $n = 3$ ;  $p \leq 0.005$ ; [Figure 4G](#)). These data confirm that SPN neurons have large voltage-gated calcium currents, and the voltage-dependent inactivation of  $I_{TCa}$  (gray shaded area in [Figures 4B](#) and [4D](#)) suggests that IPSPs would promote recovery from inactivation. So what is the more important role for the IPSP: activation of  $I_H$  or deinactivation of  $I_{TCa}$ ?

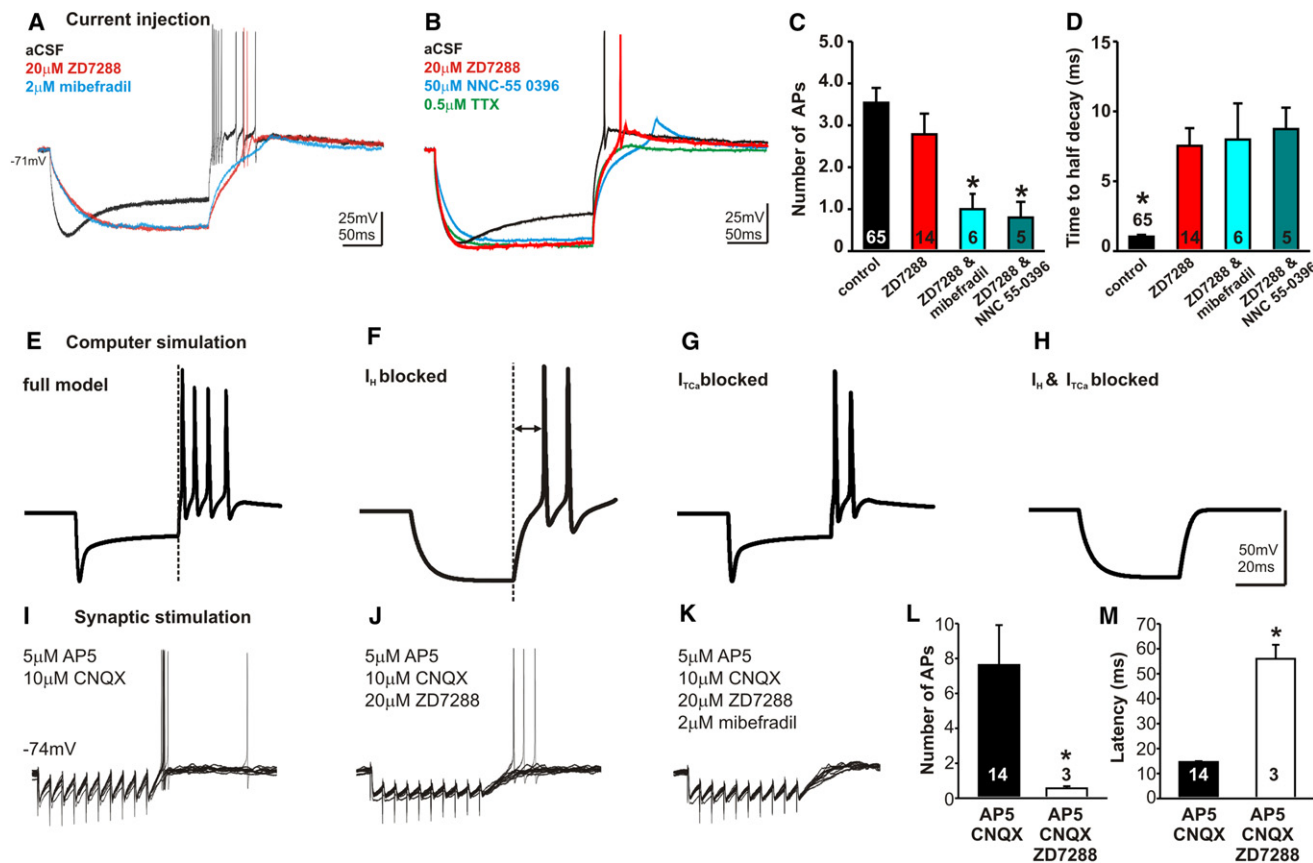


**Figure 5. SPN Offset APs Are Primed by Hyperpolarizing Current Injection or IPSPs and Mediated by  $I_H$  with Contributions from  $I_{TCa}$**   
(A and B) Hyperpolarization of two SPN neurons (−400 pA; 200 ms) generates short-latency offset firing under control conditions (black traces) but the latency increases and the number of offset APs declines after perfusion of ZD7288 (20  $\mu$ M, red traces). Additional application of mibefradil (blue trace in A) or NNC-550396 (blue trace in B) caused failure of the offset AP firing. In some cases a small subthreshold offset depolarization remained in the presence of these blockers, but this was suppressed by TTX (green trace).  
(C) Average data show that the number of offset APs was significantly reduced after application of ZD7288 and a T-type calcium channel antagonist (mibefradil or NCC-55 0396).  
(D) The remaining offset APs in the absence of  $I_H$  (i.e., following ZD7288) are delayed due to a large increase in the membrane time constant, measured as the time to half decay. Mibefradil or NCC-55 0396 did not introduce further delays.  
(E) Identical offset firing was generated by current injection in a Hodgkin-Huxley model of an SPN neuron.  
(F) Deletion of  $I_H$  alone increased the input resistance, slowed the membrane time constant, and delayed offset firing (arrow).  
(G) Deletion of  $I_{TCa}$  alone reduced the number of offset APs but had little effect on the latency to offset APs.  
(H) Without both  $I_H$  and  $I_{TCa}$ , no offset APs are generated.  
(I) Returning to in vitro SPN recordings, offset responses are triggered by synaptic stimulation of the inhibitory input with excitatory transmission blocked.  
(J) Application of ZD7288 caused a similar increase in offset AP latency to that seen in (A) and (F).  
(K) Again, additional application of mibefradil further diminished the offset response.  
(L and M) Quantification confirmed that IPSP activation of offset firing gave similar results to those obtained with current injections (shown in parts A–D). n is indicated in each bar graph; \*p < 0.05, Student's t test.

### $I_H$ and $I_{TCa}$ Have Distinct Contributions to the Offset Response

The combined results from our in vivo and in vitro recording demonstrate that sound activation of IPSPs hyperpolarizes the membrane potential, activates  $I_H$ , and removes  $I_{TCa}$  inactivation. Under current-clamp recording conditions, application of an  $I_H$  antagonist (ZD7288, 20  $\mu$ M) slowed the membrane time constant and removed the voltage “sag” (Figures 5A and 5B, red trace). This block of  $I_H$  slowed the time to half-decay from  $1.03 \pm 0.1$  ms to  $7.53 \pm 1.3$  ms (n = 14; p ≤ 0.001; Figure 5D). Blockade

of  $I_{TCa}$  by mibefradil or NNC 55-0396 did not further influence the timing of the offset response (Figures 5A and 5B) but it reduced the number of offset APs from  $3.5 \pm 1.3$  (control; n = 65) to  $1.0 \pm 0.4$  (mibefradil; n = 6; p = 0.009) or  $0.8 \pm 0.3$  (NNC 55-0396; n = 5; p = 0.008; Figures 5A, 5B, and 5D). However, even the blockade of both  $I_H$  and  $I_{TCa}$  did not further change the membrane time constant or time to half-decay (Figure 5C; n = 11; p = 0.69), consistent with the idea that  $I_H$  is the dominant current for driving short-latency offset firing. The subthreshold depolarization that remained after blocking  $I_H$  and  $I_{TCa}$  was TTX sensitive (Figure 5B,

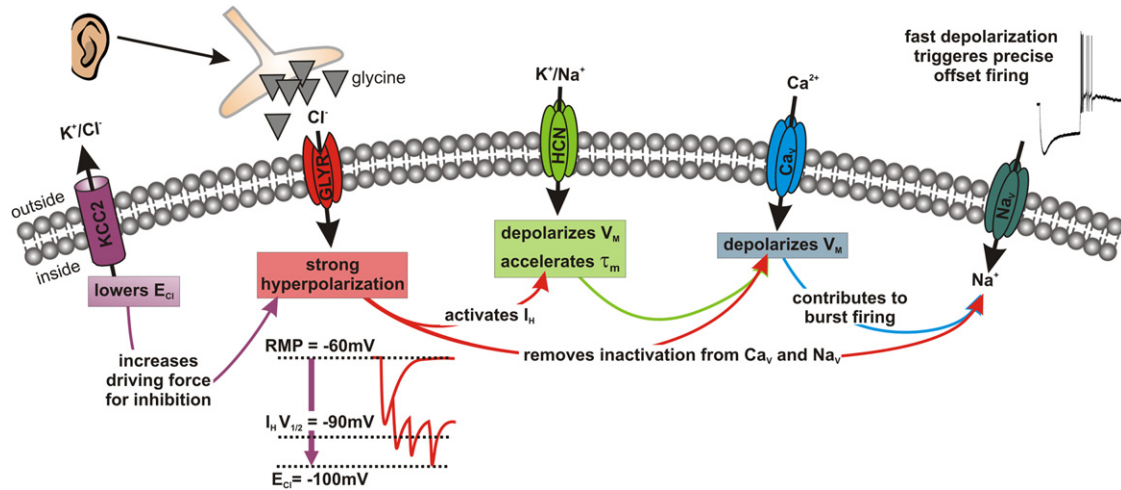


**Figure 6. Summary Illustration of the Interactions between  $E_{Cl}$ , IPSP,  $I_H$ , and  $I_{T_{Ca}}$  in Generating Offset Firing**

Sound activates glycinergic inhibition in the SPN. Due to high KCC2 activity the driving force for the IPSP is large and the membrane potential approaches  $E_{Cl}$ . This activates a substantial proportion of the  $I_H$  conductance and removes steady-state inactivation of  $Na_v$  and  $I_{T_{Ca}}$ . After cessation of the inhibition, the depolarizing conductances generate a burst of well-timed offset APs.

green trace). As a further test of our hypothesis we developed a computational model of SPN neuron firing, in which we could test the ionic basis of offset firing and separate the relative importance and contributions of  $I_H$  and  $I_{T_{Ca}}$ . The basic Hodgkin-Huxley model could match the control firing pattern, AP waveform, and activation of offset APs in response to hyperpolarizing current injection (Figure 5E). Upon removal of  $I_H$ , offset APs were evoked at longer latencies, confirming that this conductance is crucial for the fast-membrane time constant and the short-latency offset firing (Figure 5F). Removal of the  $I_{T_{Ca}}$  conductance also compromised offset firing, in that fewer APs were triggered (Figure 5G) but their latency remained as short as in the full model. Removal of both  $I_H$  and  $I_{T_{Ca}}$  (Figure 5H) confirmed that both conductances were necessary for the full physiological offset phenotype, with  $I_H$  being the dominant conductance for the short-latency offset AP, while  $I_{T_{Ca}}$  generated a slower depolarization, which increased the number of longer-latency offset APs. To test this hypothesis in response to a physiological input, we used repetitive IPSPs evoked by electrical stimulation of the MNTB in vitro (Figure 5I; 100 Hz train for 100 ms) and consecutively applied ZD7288 and mibefradil. After bath application of ZD7288 (20  $\mu$ M; 20 min) the membrane time constant slowed, offset firing declined, and latencies increased (Figure 5J). Additional perfusion of mibefradil (2  $\mu$ M) further suppressed offset firing (Figure 5K). Changes in the number and timing of offset firing were similar to the respective changes observed with current injections (Figures 5L and 5M).  $I_H$  and  $I_{T_{Ca}}$  modify offset firing in response to either current injections or IPSP activation, confirming that both conductances are physiologically relevant. This result emphasizes that the combination of a negative chloride reversal potential, a strong inhibitory input, and the subsequent activation of intrinsic conductances are important for the physiological function of the SPN neurons in generating offset APs, marking the termination of a sound (Figure 6).

### Physiological Impact: $I_H$ Increases the Temporal Accuracy of Offset Firing

The output of the MNTB-SPN circuit into the auditory midbrain (IC) provides specific information for sound duration computation. Single-unit recordings in vivo show that MNTB principal neurons fire APs with short interspike intervals throughout any duration of sound stimulation and also showed that this is separated from ongoing spontaneous activity by a poststimulus suppression period of almost 50 ms (Kopp-Scheinflug et al., 2008; Figure 7A). SPN recordings showed increasing numbers of APs in the offset response with increasing stimulus duration in vivo (similar to rat SPON (Kadner et al., 2006); Figure 7B) and also in vitro (Figure 7C) and consistent with increased availability of  $I_{T_{Ca}}$ . For the shortest intervals (10 ms, Figure 7C, lower trace), offset firing resembled SPN responses after blocking  $I_H$  (Figure 5), emphasizing the importance of this conductance for encoding stimulus durations in the SPN and suggesting that the minimum encodable duration will be set by the activation kinetics of the  $I_H$  conductance. Indeed, recordings from HCN1 knockout mice (Figure 7C red traces) revealed HCN2-dominated, slow-membrane time constants and a vastly reduced ability to detect short intervals, with a minimum stimulus duration of 100 ms being required to trigger an offset AP.

Closer examination of MNTB AP timing shows a tight distribution of onset latencies (gray histogram; Figure 7D) but very broadly distributed timing of the last APs in the sound-evoked response (open histogram), consistent with the idea that the end of an excitatory response cannot provide accurate timing information. On the other hand the AP latency in the SPN offset response showed very little jitter (black histogram; Figure 7D); indeed, the temporal resolution of the SPN offset response is comparable to the onset response in the MNTB (Figure 7E). Thus from a computational viewpoint, the conversion of the inhibitory input to an excitatory offset response improves the temporal resolution of the encoded signal by at least 5-fold.

This result provides insight as to why conversion of the inhibitory MNTB output into an excitatory offset response gives a physiological advantage in terms of temporal accuracy of the offset, and this is confirmed by the modeling (Figures 7F–7H).

The model provides several additional insights into the physiology of offset firing. In the full SPN model, the range of sound durations is represented by a color spectrum from red (long, 100 ms) to blue (short, 10 ms) and the latency of the offset response closely matched in vivo and in vitro stimulus durations (Figures 7Fi and 7G). But removal of the  $I_H$  conductance (no  $I_H$ , green; Figure 7Fii) vastly degrades the offset timing, so that latencies increased to over 30 ms (Figure 7G). Lack of  $I_H$  also increased the input resistance so that the current step now caused a much deeper hyperpolarization, increasing recovery of other conductances (i.e.,  $I_{TCa}$  and  $Na_V$ ) from voltage-dependent inactivation, so the injected current (no  $I_H$ ,  $V_m$  corrected; Figure 7Fiii) was reduced to match the same steady-state hyperpolarization as in Figure 7Fi (dashed line). Under these conditions  $I_{TCa}$  generates a small suprathreshold offset-depolarization and a single AP for only the longest duration (100 ms, green triangle; Figure 7G), confirming that  $I_{TCa}$  is not the major trigger of offset firing. This is emphasized in the last model condition, where only  $I_{TCa}$  is deleted, and  $I_H$  alone generated a powerful short-latency single-offset response AP (Figures 7Fiv and 7G). While  $I_H$  predominates in triggering the offset response, a plot of AP number against stimulus duration (Figure 7H) emphasizes that  $I_{TCa}$  is necessary to maintain the multiple AP firing phenotype.

## DISCUSSION

Our results demonstrate a neat ionic mechanism for accurate detection of sound termination. Integration of acoustically driven synaptic inputs with intrinsic conductances converts an inhibition into a well-timed AP offset response by which sound termination and gaps in ongoing sounds are encoded. Sound-evoked inhibition generates large IPSPs in the SPN, which because of the extreme negative  $E_{Cl}$  can drive  $I_H$  activation (accelerating the neuronal membrane time constant) and remove steady-state inactivation of  $I_{TCa}$  so that on termination of the sound, rapid repolarization triggers a short-latency burst of APs. The primary drive for AP firing is  $I_H$ , although  $I_{TCa}$  (as well as  $Na_V$ ,  $Kv1$ , and  $Kv3$  currents) influence the number and timing of offset APs. The Hodgkin-Huxley modeling confirmed dominance of  $I_H$  in translating IPSPs into an excitatory output. This computation generates an “inversion” of the inhibitory input to give offset firing on sound termination with enhanced timing accuracy (of equivalent accuracy to the onset response) and forms part of the sound duration processing in the auditory midbrain.

### Offset Firing Is Mediated by Intrinsic Conductances

Small-amplitude EPSPs can be evoked in the SPN in vitro, but the results show that EPSPs are not the primary drive for offset firing (for example, through EPSPs outlasting the inhibition). Offset firing was evoked in the absence of synaptic stimulation (via current-injection) and also occurred when evoked by IPSPs (on stimulation of the MNTB) in the presence of glutamate receptor antagonists. We can also exclude the hypothesis that the chloride reversal potential ( $E_{Cl}$ ) becomes more positive

than the RMP, since in fact the opposite is happening: large IPSPs are generated because  $E_{Cl}$  is so negative (–100mV) and as reported previously (Löhrke et al., 2005). This is an important result as it explains how  $I_H$  can be activated by sensory stimuli under physiological conditions.

### Conjunction of $I_H$ with $I_{TCa}$ Is Associated with Rhythm Generation

$I_H$  currents are activated by hyperpolarization with half-activation voltages of –70mV to –95mV for HCN1- and HCN2-dominated channels, respectively (Wahl-Schott and Biel, 2009). They mediate an important role in setting the resting membrane potential (Cuttle et al., 2001; Nolan et al., 2007; Seifert et al., 1999; Wang et al., 2002) and in integrating dendritic EPSPs (Berger et al., 2001; Nolan et al., 2004, 2007). In conjunction with  $I_{TCa}$ ,  $I_H$  channels contribute to membrane potential oscillations and rhythm generation (McCormick and Pape, 1990; Soltesz et al., 1991) in thalamocortical (Steriade et al., 1993) and cerebellar networks (Llinás and Mühlethaler, 1988) and to rhythm generation in the heart (Wahl-Schott and Biel, 2009).

In general, voltage-clamp quality declines with distance along the dendrites from a somatic recording site (space clamp) as derived from the elegant cable theories of Wilfred Rall (see Rall et al., 1992; Williams and Mitchell 2008). In contrast to cortical pyramidal neurons where  $I_H$  is most highly expressed in distal dendrites (Berger et al., 2001), HCN1 channels in the SPN have a somatic and proximal location, as confirmed by immunohistochemistry. This permits good voltage clamp of this conductance and favors the physiological role in minimizing the latency to triggering fast rebound AP firing through proximity to the axon and spike initiation sites.

The phenomenon of “post-inhibitory rebound” occurs in the basal ganglia, thalamus, cerebellum and hippocampus. It is loosely defined as enhanced firing following hyperpolarization during rhythmic firing, and attributed to  $I_H$  and  $I_{TCa}$  currents (Aizenman and Linden, 1999; Cooper and Stanford, 2000). However, rebound firing has heterogeneous ionic mechanisms that may be dominated by  $I_H$  and/or  $I_{TCa}$  conductances, and result from after-hyperpolarization (AHP, driven by  $E_K$ ) following an AP or IPSPs (driven by  $E_{Cl}$ ) depending on the cell type under study. Additional contributions could also arise from the enhanced recovery of voltage-gated  $Na^+$  channels from inactivation (Aman and Raman, 2007). Rebound firing in direct response to synaptic inhibition has been proposed (and is widely accepted as an obvious mechanism) but it has rarely been demonstrated (Nambu and Llinas, 1994) particularly in response to physiological sensory stimulation in the mammalian CNS. Recent studies employing synaptic stimulation were unable to demonstrate physiological rebound firing in the deep cerebellar nuclei (Alviña et al., 2008). In songbirds rebound firing has been linked with vocal learning, where thalamic neurons translate IPSPs into an excitatory output (Bottjer, 2005; Person and Perkel, 2005) and modeling studies clearly show the potential for  $I_H$  to generate rebound firing in the mammalian brain, but the key physiological question is: how can a physiological input sufficiently activate  $I_H$  to generate this firing? Here we show that the SPN uses powerful chloride extrusion to extend the physiological voltage range negative to  $E_K$ . This enhances the chloride driving force of IPSPs,

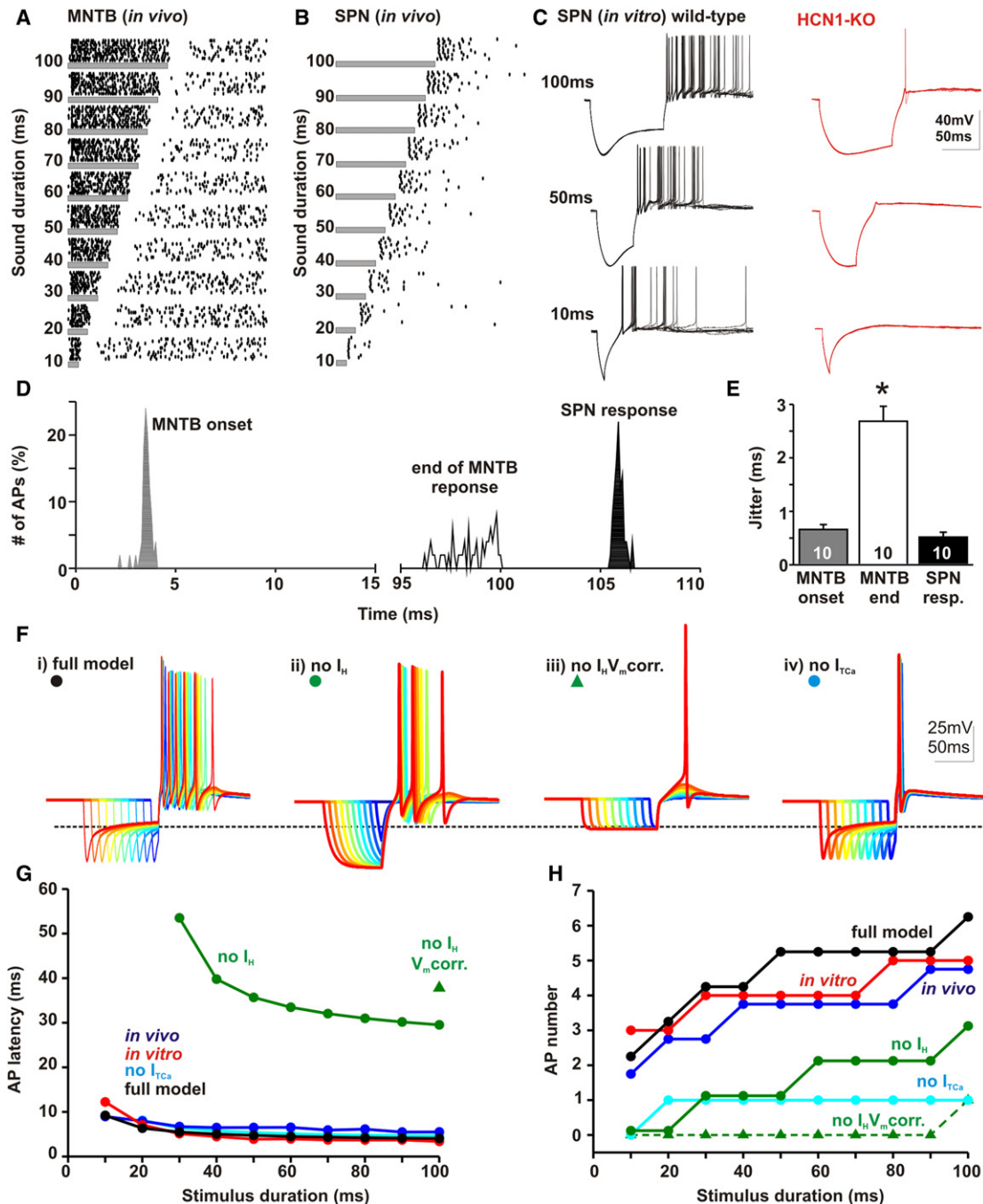


**Figure 7. The SPN Offset Firing Carries Information about Sound Duration and Has Improved Temporal Encoding Compared to the Offset Latency of the Input, from the MNTB**

(A) In vivo MNTB: dot raster plot showing sound-evoked responses to increasing sound durations from 10 to 100 ms (ten repetitions each).  
 (B) In vivo SPN: dot raster plot showing an offset response to sound durations from 10 to 100 ms.  
 (C) In vitro SPN: offset responses measured in current clamp during hyperpolarizing current injection (−400 pA) for 100 ms, 50 ms, and 10 ms durations in WT (black traces) and HCN1-KO (red traces).  
 (D) Histograms showing the distribution of AP latencies in response to 50 repetitions of a 100 ms tone (CF/80 dB SPL) for the first onset AP (gray) and the last sound-driven AP (open) of an MNTB neuron compared to the first offset AP (black) of an SPN neuron.  
 (E) The accuracy of the SPN offset firing matches that of the MNTB onset seen in (D). Jitter is taken as the standard deviation of first/last spike latency for 50 stimulus repetitions (CF, 80 dB SPL, 100 ms, 5 ms ramps).  
 (F) The SPN Hodgkin-Huxley model shows overlaid current-clamp traces with different hyperpolarization durations ranging from 10 to 100 ms, color coded from blue to red, respectively. (i) Full model. (ii) Deletion of  $I_H$ . (iii) Deletion of  $I_H$  with membrane potential correction. (iv) Deletion of  $I_{TCA}$ .

which can then provide sufficient hyperpolarization to activate the  $I_H$  conductance.

### Physiological Relevance of $I_H$ in the Auditory System

$I_H$  has a general role in modulating input resistance and hence the membrane time constant; this is especially important in the auditory system, which depends on speed and temporal precision (Bal and Oertel, 2000; Oertel et al., 2008). Although sound localization mechanisms accurately discriminate submillisecond time intervals (McAlpine et al., 2001), the MNTB-SPN circuit forms an early computation adapted to encode millisecond to second time intervals. The idea that  $I_H$  could be involved in this computation was first proposed from the modeling studies of Hooper et al. (Hooper et al., 2002), who suggested different cell categories (low-pass, band-pass, or high-pass) to encode sound of different durations, but all limited to sounds lasting longer than 50 ms. For instance, induction of offset responses in the IC by 200 ms hyperpolarizing current injections was mediated by  $I_H$  (Koch and Grothe, 2003), while 50 ms sound pulses failed to do so in the same nucleus (Xie et al., 2007). However, encoding derives not only from stimulus duration but also from “intensity,” since loud sounds with higher input firing rates will generate greater summation of IPSPs and activate more  $I_H$  current. Therefore, a short-duration sound could elicit an offset response if delivered at a higher intensity, and provided the activation kinetics of  $I_H$  were fast enough. Coincidence-based modeling of IPSPs and EPSPs (Aubie et al., 2009) can provide duration tuning at short intervals, but this mechanism is not used in the SPN (our results) nor in the thalamus of songbirds (Person and Perkel, 2005) where excitatory transmission is also not required to generate an offset response. Many *in vitro* studies of  $I_H$  kinetics have been conducted at room temperature, and so activation rates are slower than *in vivo*, but our empirical observations at physiological temperatures demonstrate that the faster kinetics of HCN1 in the SPN can encode durations even shorter than 10 ms. Indeed, the shortest stimulus duration observed that generated an offset AP in this study was 6 ms, although this is too short to activate sufficient  $I_H$  for short-latency offset firing. This could also explain why in the SPN, amplitude modulated tones are encoded with high vector strength up to about 200 Hz, but phase-locking declines as soon as the period length drops below 5–10 ms (Kadner and Berrebi, 2008). The apparent inability to encode short durations does not limit the impressive performance in gap detection tests in the same study (Kadner and Berrebi, 2008). This is because successful gap detection, which is a major cue for vocal communication (Walton, 2010), crucially depends on the sound duration prior to the gap (Person and Perkel, 2005) rather than with the duration of the gap itself. This is consistent with the time required to activate  $I_H$  (as seen with the “sag” under current clamp) and to remove steady-state inactivation of  $I_{Tca}$ . The minimal gap in a stimulus train that can be detected by our model is  $2.12 \pm 0.58$  ms for

a 200 ms pregap duration (Figures 8A and 8C). Shorter pregap durations (less than 50 ms) will not activate sufficient  $I_H$  and although offset APs can be generated with much shorter stimuli (see above), their latency is too slow to appear within a short gap, and so will be suppressed by the incoming train of IPSPs from the following sound (Figures 8B and 8C). Reducing the  $I_H$  conductance by 50% to imitate the HCN1 knockout data or shifting  $E_{Cl}$  by 20mV more positive causes gap thresholds to double or triple, respectively (Figure 8D). Given that vocalizations in small rodents last between 20 ms and several hundred milliseconds (rat: Brudzynski et al., 1993; mouse: Holmstrom et al., 2010), the mechanism we propose here is well suited to encode the duration of stimuli used in species-specific communication.

Although duration-sensitive neuronal responses have been described in the auditory midbrain (Covey and Casseday, 1999) the origin and mechanism of this duration tuning is unknown. The powerful offset response of rat SPON neurons (Kadner et al., 2006) is confirmed here in mouse SPN and our voltage-clamp studies further establish the SPN/SPON as the site for offset tuning. Convergence of SPN/SPON offset encoding with VNLL onset responses in the IC could provide the inputs for “on-off” cells in the auditory midbrain (Saldaña et al., 2009; Pollak et al., 2011). However, an important function of this SPN offset firing is to match the timing accuracy of sound termination with that of the sound onset, as compared here for the MNTB (Figures 7D and 7E). While excitatory projections are well adapted for onset temporal accuracy, the termination of a sensory response is ambiguous because of adaptation, spontaneous activity, and the decay of the EPSP (or IPSP)—a problem that is solved by acceleration of the membrane time constant with  $I_H$  as described in the present study. From a signal-processing viewpoint it is advantageous to encode the envelope of a complex signal by equivalently accurate onsets and offsets, since this doubles the sampling rate and increases temporal resolution.

Offset responses are considered to be of important physiological significance for perceptual grouping (Plack and White, 2000). However, these responses are not generated within the auditory cortex (Scholl et al., 2010), suggesting that the mechanism is further upstream. Here, we demonstrate *in vivo* and *in vitro* that the interplay of a negative chloride reversal potential, a strong inhibition and a powerful  $I_H$  results in a temporally precise, duration-sensitive offset response in the SPN.

## EXPERIMENTAL PROCEDURES

### In Vitro Preparations

CBA/Ca mice and HCN1 knockout mice (P14–P21) were killed by decapitation in accordance with the UK Animals (Scientific Procedures) Act 1986 and brainstem slices containing the superior olivary complex (SOC) prepared as previously described (Johnston et al., 2008). Transverse slices (200- $\mu$ m-thick) containing the SPN were cut in a low-sodium artificial CSF (aCSF) at  $\sim 0^\circ\text{C}$ . Slices were maintained in a normal aCSF at  $37^\circ\text{C}$  for 1hr, after which

(G)  $I_H$  is crucial for a short latency first spike and is shown for each of the above conditions: *in vivo*, *in vitro*, and full model. The latency of the offset response declines from about 10 ms to about 3 ms for respective durations from 20 to 100 ms for all the conditions, except that without  $I_H$  (green trace) where the latency is vastly extended to over 30 ms across all the durations.

(H) There are increasing numbers of APs for increasing durations for *in vivo*, *in vitro*, and the full model. The number of offset APs increased with increasing stimulus duration, but in the absence of  $I_{Tca}$  only a single offset spike is generated (light blue trace).

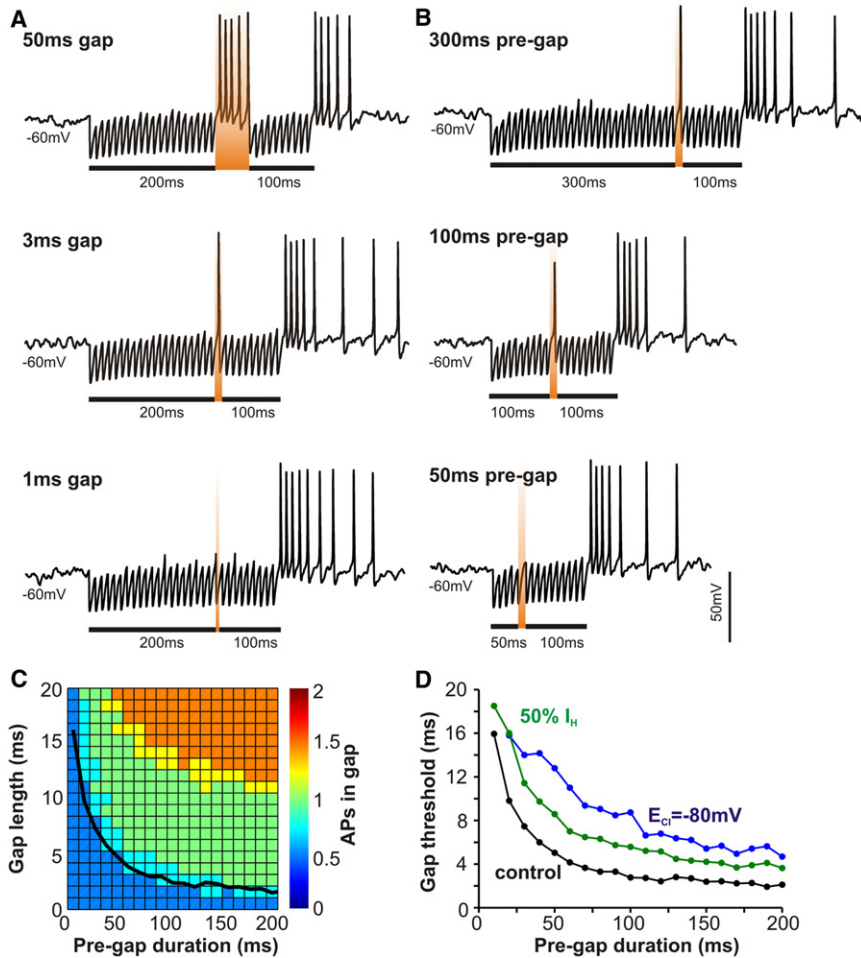


**Figure 8. A Large  $I_H$  and Very Negative  $E_{Cl}$  Account for Low-Threshold Gap Detection**

The SPN model using the observed levels of intrinsic conductances can account for physiological limits of gap detection.

(A) A stimulus train of 200 ms (100 Hz IPSPs) is interrupted by an interval containing no stimulation (i.e., a gap, silence, indicated by the orange shaded region in each trace). This gap is detected by the SPN intrinsic conductances and encoded by an offset AP for gap durations of 50 ms (upper trace) and 3 ms (middle trace) but not for a 1 ms gap (lower trace).

(B) The duration of the pregap stimulus influences the threshold for gap detection. A 3 ms gap following a pregap duration of 300 ms (upper trace) or 100 ms (middle trace) is detected by a single AP; however, a 3 ms gap is not detected following a stimulus lasting only 50 ms (lower trace).

(C) Gap length is plotted versus pregap duration. Gap threshold (black line, defined as 50% firing probability) is the average minimal gap from 20 trials. The ability of the SPN neurons to detect the gap increases with the pregap duration, consistent with the kinetics of  $I_H$  activation.

(D) Minimal gap thresholds are observed following longer pregap durations. Gap detection requires short-latency offset firing mediated by a large IPSP and  $I_H$ , accordingly, gap thresholds are elevated either if  $I_H$  is reduced by 50% (green line) or if  $E_{Cl}$  is shifted by 20mV toward more positive potentials (blue line).

they were stored at room temperature ( $\sim 20^\circ\text{C}$ ) in a continually recycling slice-maintenance chamber. For composition of solutions please see Supplemental Experimental Procedures. Experiments were conducted at a temperature of  $36^\circ\text{C} \pm 1^\circ\text{C}$  using a Peltier driven environmental chamber (constructed by University of Leicester Mechanical and Electronic Joint Workshops) or using a CI7800 (Campden Instruments, UK) feedback temperature controller.

#### Patch Clamp

Whole-cell patch-clamp and current-clamp recordings were made from visually identified SPN neurons (Figure S2; Nikon FN600 microscope with differential interference contrast optics) using a Axopatch 200B amplifier (Molecular Devices, Sunnyvale, CA, USA) and pClamp10 software (Molecular Devices), sampling at 50 kHz and filtering at 10 kHz. Patch pipettes were pulled from borosilicate glass capillaries (GC150F-7.5, OD: 1.5 mm; Harvard Apparatus, Edenbridge, UK) using a two-stage vertical puller (PC-10 Narishige, Tokyo, Japan). Their resistance was  $\sim 3.0\text{ M}\Omega$  when filled with a patch solution containing (mM): KGlucuronate 97.5, KCl 32.5, HEPES 40, EGTA 5,  $\text{MgCl}_2$  1,  $\text{Na}_2\text{phosphocreatine}$  5; pH was adjusted to 7.2 with KOH.

For the calcium current measurements,  $I_{\text{Tca}}$  was recorded as described above, using a different rig with pClamp10 software (Molecular Devices), sampling at 10 kHz and filtering at 5 kHz. The pipette solution contained (mM): CsCl 120, NaCl 10, TEACl 10, EGTA 1, HEPES 40,  $\text{Na}_2\text{phosphocreatine}$  5, QX314 2, ZD2788 0.02; 2 mM ATP and 0.5 mM GTP were added on the day of use. The composition of the external solution was (mM): NaCl 95,  $\text{NaHCO}_3$  26.2, TEACl 30, KCl 2.5, glucose 10,  $\text{NaH}_2\text{PO}_4$  1.25, ascorbic acid 0.5,  $\text{MgCl}_2$  1.3,  $\text{CaCl}_2$  2, Bicuculline 0.01, Strychnine 0.001. For

stimulus trains evoked using a DS2A isolated stimulator ( $\sim 1\text{--}10\text{V}$ , 0.2 ms; Digitimer, Welwyn Garden City, UK).

#### In Vivo Recordings

These experiments were performed at the V.M. Bloedel Hearing Research Center of the University of Washington in Seattle (USA). All experimental procedures were approved by the University of Washington Institutional Animal Care and Use Committee and were performed in accordance with the NIH guideline for the Care and Use of Laboratory Animals. Spontaneous and evoked MNTB and SPN neuron responses were recorded from 6 mice (CBA/Ca; P23-P54; see Supplemental Experimental Procedures for details), which were anesthetized by intraperitoneal injection of a mixture of ketamine hydrochloride (100 mg/kg BW) and xylazine hydrochloride (5 mg/kg BW). MNTB single-unit recordings characteristically possess a prepotential, followed by a biphasic postsynaptic action potential and responded to sound from the contralateral ear (Kopp-Scheinflug et al., 2003). SPN recordings were obtained from recording sites located dorsolaterally to the MNTB. Single units in the SPN were typically characterized by a low spontaneous firing rate and broad frequency tuning. For retrograde tracing experiments, 2  $\mu\text{l}$  fluorogold were pressure injected into the inferior colliculus of anesthetized mice using a stereotaxic device. After 5–7 days recovery period, animals were sacrificed and brain sections taken for subsequent fluorescent microscopy (see below).

#### Immunohistochemistry

Brainstems were dissected from P16 wild-type and HCN1 knockout littermates, which had been killed by decapitation (as above) and were frozen in

calcium current measurements a junction potential of  $-4.1\text{mV}$  ( $\sim 4\text{mV}$ ) was subtracted.

Synaptic responses were evoked with a bipolar platinum electrode placed across the MNTB and

LAMB OCT compound (ThermoFisher Scientific) prior to cryostat sectioning (Microm HM 560) at 12  $\mu\text{m}$  in the transverse plane. Sections were fixed in 4% paraformaldehyde at 4°C for 25 min and subsequently incubated for 60 min at room temperature with PBS containing 0.1% Triton X-100 (PBS-T), 1% BSA, and 10% normal goat serum (NGS) to reduce nonspecific binding of secondary antibody. Sections were incubated with primary antibodies to HCN1 (1:500, Alomone) or HCN2 (1:1000, Alomone) and colabeled with KCC2 (1:1000, Millipore), all diluted in PBS-T containing 1% BSA and 10% NGS overnight at 4°C. After three washes in PBS-T, sections were incubated with the secondary antibodies (Invitrogen; AlexaFluor 488 goat anti-rabbit IgG and AlexaFluor 546 goat anti-mouse IgG [1:1000]) diluted in PBS-T, 1% BSA, and 10% NGS for 2 hr at room temperature. After rinsing in PBS-T, sections were coverslipped with Vectashield Hard Set Mounting Medium with DAPI (Vector Laboratories) and images were acquired with a Zeiss laser-scanning confocal microscope (LSM 510, Carl Zeiss International) or Leica DM2500 fluorescence microscope. As negative controls for specificity, sections incubated with the omission of the primary antibody showed no specific immunolabeling (data not shown).

### Computational Model

A simple, single-compartment model of a prototypical SPN neuron was simulated using NEURON (version 7.1, Hines and Carnevale, 2001). The neuron was implemented as a single cylindrical compartment 15.5  $\mu\text{m}$  in length and 15.5  $\mu\text{m}$  in diameter. Specific membrane capacitance was  $c_m = 2\text{mF}/\text{cm}^2$ . The following conductances were included: a leak conductance (reversal potential  $E_{\text{leak}} = -90\text{mV}$ ), a  $\text{Na}^+$  conductance, low- and high-voltage-activated K $^+$  conductances, a hyperpolarization-activated conductance ( $I_{\text{h}}$ ), and a low-threshold voltage-activated  $\text{Ca}^{2+}$  conductance ( $I_{\text{TCa}}$ ). In this model the resting potential is primarily determined by a tonically active  $I_{\text{h}}$ . A full description of the conductances with all parameters is given in the Supplemental Experimental Procedures. To directly reproduce the in vitro experiments, the model neuron was stimulated with current injections of different magnitude.

In some simulations, noise was added as an EPSC conductance to simulate random synaptic events. Fluctuations were modeled as an Ornstein-Uhlenbeck process with a mean conductance  $g_n = 1$  pS, standard deviation  $\sigma_n = 0.5$  nS, and reversal potential  $E_{\text{rev,Exc.}} = 0\text{mV}$ . The numerical integration scheme introduced by Rudolph and Destexhe (2005) was used in all simulations. Inhibitory synapses were modeled by a two-state kinetic model (Neuron's Exp2Syn) with rise time constant  $\tau_1 = 0.1$  ms, decay time constant  $\tau_2 = 2$  ms, and reversal potential  $E_{\text{rev,Inh}} = -100\text{mV}$ . In all simulations, the neuron had 14 inhibitory synapses, each with a peak conductance of 4 nS. The model code is available at ModelDB (<https://senselab.med.yale.edu/modeldb/ShowModel.asp?model=139657>); accession number 139657.

### Data Analysis and Statistical Methods

Statistical analyses of the data were performed with SigmaStat/SigmaPlot (SPSS Science, Chicago, IL). Results are reported as mean  $\pm$  SEM,  $n$  being the number of neurons recorded from at least 3 different animals. Statistical comparisons between different data sets were made using unpaired Student's  $t$  test. Differences were considered statistically significant at  $p < 0.05$ . Activation kinetics of  $I_{\text{h}}$  currents and T-type  $\text{Ca}^{2+}$  currents were determined fitting a Boltzmann function through the respective tail currents:

$$I(V) = \frac{1}{1 + \frac{\exp(V_{0.5,\text{act}} - V_m)}{k}}$$

Where  $I(V)$  is the normalized current,  $V_m$  is the clamped membrane potential,  $V_{0.5,\text{act}}$  is the membrane potential where half the channels are open, and  $k$  is the slope factor for activation.

### ACCESSION NUMBER

The code of the computational model is available under accession number at ModelDB: <https://senselab.med.yale.edu/modeldb/ShowModel.asp?model=139657>.

### SUPPLEMENTAL INFORMATION

Supplemental Information includes four figures and Supplemental Experimental Procedures and can be found with this article online at doi:10.1016/j.neuron.2011.06.028.

### ACKNOWLEDGMENTS

This work was supported by the Medical Research Council, UK, MRC Fellowship G0900425 (M.H.), and NIH DC002793 (B.T.). We are grateful to Matt Nolan and Derrick Garden for providing the HCN1 knockout mice and thank Sarah J. Griffin for initial implementation of our Neuron models. Author contributions: C.K.-S., conducted experiments, analyzed and interpreted data, and jointly wrote the manuscript; A.J.B.T. conducted calcium current experiments; S.W.R. conducted immunohistochemistry; B.L.T. supported and advised on in vivo experiments; M.H.H. developed the computational model in consultation with I.D.F. and C.K.-S.; and I.D.F. conceived of the project jointly with C.K.-S., designed experiments, interpreted data, and jointly wrote the manuscript.

Accepted: June 13, 2011

Published: September 7, 2011

### REFERENCES

- Aizenman, C.D., and Linden, D.J. (1999). Regulation of the rebound depolarization and spontaneous firing patterns of deep nuclear neurons in slices of rat cerebellum. *J. Neurophysiol.* 82, 1697–1709.
- Alviña, K., Walter, J.T., Kohn, A., Ellis-Davies, G., and Khodakhah, K. (2008). Questioning the role of rebound firing in the cerebellum. *Nat. Neurosci.* 11, 1256–1258.
- Aman, T.K., and Raman, I.M. (2007). Subunit dependence of Na channel slow inactivation and open channel block in cerebellar neurons. *Biophys. J.* 92, 1938–1951.
- Aubie, B., Becker, S., and Faure, P.A. (2009). Computational models of millisecond level duration tuning in neural circuits. *J. Neurosci.* 29, 9255–9270.
- Bal, R., and Oertel, D. (2000). Hyperpolarization-activated, mixed-cation current ( $I_{\text{h}}$ ) in octopus cells of the mammalian cochlear nucleus. *J. Neurophysiol.* 84, 806–817.
- Banks, M.I., and Smith, P.H. (1992). Intracellular recordings from neurobiotin-labeled cells in brain slices of the rat medial nucleus of the trapezoid body. *J. Neurosci.* 12, 2819–2837.
- Barnes-Davies, M., Barker, M.C., Osmani, F., and Forsythe, I.D. (2004). Kv1 currents mediate a gradient of principal neuron excitability across the tonotopic axis in the rat lateral superior olive. *Eur. J. Neurosci.* 19, 325–333.
- Behrend, O., Brand, A., Kapfer, C., and Grothe, B. (2002). Auditory response properties in the superior paraolivary nucleus of the gerbil. *J. Neurophysiol.* 87, 2915–2928.
- Berger, T., Larkum, M.E., and Lüscher, H.R. (2001). High  $I_{\text{h}}$  channel density in the distal apical dendrite of layer V pyramidal cells increases bidirectional attenuation of EPSPs. *J. Neurophysiol.* 85, 855–868.
- Bottjer, S.W. (2005). Timing and prediction the code from basal ganglia to thalamus. *Neuron* 46, 4–7.
- Budzynski, S.M., Bihari, F., Ociepa, D., and Fu, X.W. (1993). Analysis of 22 kHz ultrasonic vocalization in laboratory rats: long and short calls. *Physiol. Behav.* 54, 215–221.
- Cooper, A.J., and Stanford, I.M. (2000). Electrophysiological and morphological characteristics of three subtypes of rat globus pallidus neurone in vitro. *J. Physiol.* 527, 291–304.
- Covey, E., and Casseday, J.H. (1999). Timing in the auditory system of the bat. *Annu. Rev. Physiol.* 61, 457–476.
- Cuttle, M.F., Rusznák, Z., Wong, A.Y., Owens, S., and Forsythe, I.D. (2001). Modulation of a presynaptic hyperpolarization-activated cationic current

- (Ih) at an excitatory synaptic terminal in the rat auditory brainstem. *J. Physiol.* 534, 733–744.
- Dehmel, S., Kopp-Scheinflug, C., Dörrscheidt, G.J., and Rübsamen, R. (2002). Electrophysiological characterization of the superior paraolivary nucleus in the Mongolian gerbil. *Hear. Res.* 172, 18–36.
- Grothe, B., and Park, T.J. (2000). Structure and function of the bat superior olivary complex. *Microsc. Res. Tech.* 51, 382–402.
- Hines, M.L., and Carnevale, N.T. (2001). NEURON: a tool for neuroscientists. *Neuroscientist* 7, 123–135.
- Holmstrom, L.A., Eeuwes, L.B., Roberts, P.D., and Portfors, C.V. (2010). Efficient encoding of vocalizations in the auditory midbrain. *J. Neurosci.* 30, 802–819.
- Hooper, S.L., Buchman, E., and Hobbs, K.H. (2002). A computational role for slow conductances: single-neuron models that measure duration. *Nat. Neurosci.* 5, 552–556.
- Johnston, J., Griffin, S.J., Baker, C., Skrzypiec, A., Chernova, T., and Forsythe, I.D. (2008). Initial segment Kv2.2 channels mediate a slow delayed rectifier and maintain high frequency action potential firing in medial nucleus of the trapezoid body neurons. *J. Physiol.* 586, 3493–3509.
- Kadner, A., and Berrebi, A.S. (2008). Encoding of temporal features of auditory stimuli in the medial nucleus of the trapezoid body and superior paraolivary nucleus of the rat. *Neuroscience* 151, 868–887.
- Kadner, A., Kulesza, R.J., Jr., and Berrebi, A.S. (2006). Neurons in the medial nucleus of the trapezoid body and superior paraolivary nucleus of the rat may play a role in sound duration coding. *J. Neurophysiol.* 95, 1499–1508.
- Kaila, K., Lamsa, K., Smirnov, S., Taira, T., and Voipio, J. (1997). Long-lasting GABA-mediated depolarization evoked by high-frequency stimulation in pyramidal neurons of rat hippocampal slice is attributable to a network-driven, bicarbonate-dependent K<sup>+</sup> transient. *J. Neurosci.* 17, 7662–7672.
- Koch, U., and Grothe, B. (2003). Hyperpolarization-activated current (Ih) in the inferior colliculus: distribution and contribution to temporal processing. *J. Neurophysiol.* 90, 3679–3687.
- Kopp-Scheinflug, C., Fuchs, K., Lippe, W.R., Tempel, B.L., and Rübsamen, R. (2003). Decreased temporal precision of auditory signaling in Kcna1-null mice: an electrophysiological study in vivo. *J. Neurosci.* 23, 9199–9207.
- Kopp-Scheinflug, C., Tolnai, S., Malmierca, M.S., and Rübsamen, R. (2008). The medial nucleus of the trapezoid body: comparative physiology. *Neuroscience* 154, 160–170.
- Kulesza, R.J., Jr. (2008). Cytoarchitecture of the human superior olivary complex: nuclei of the trapezoid body and posterior tier. *Hear. Res.* 241, 52–63.
- Kulesza, R.J., Jr., Spirou, G.A., and Berrebi, A.S. (2003). Physiological properties of neurons in the superior paraolivary nucleus of the rat. *J. Neurophysiol.* 89, 2299–2312.
- Kuwabara, N., and Zook, J.M. (1991). Classification of the principal cells of the medial nucleus of the trapezoid body. *J. Comp. Neurol.* 314, 707–720.
- Kuwabara, N., DiCaprio, R.A., and Zook, J.M. (1991). Afferents to the medial nucleus of the trapezoid body and their collateral projections. *J. Comp. Neurol.* 314, 684–706.
- Llinás, R., and Mühlethaler, M. (1988). An electrophysiological study of the in vitro, perfused brain stem-cerebellum of adult guinea-pig. *J. Physiol.* 404, 215–240.
- Löhrke, S., Srinivasan, G., Oberhofer, M., Doncheva, E., and Friauf, E. (2005). Shift from depolarizing to hyperpolarizing glycine action occurs at different perinatal ages in superior olivary complex nuclei. *Eur. J. Neurosci.* 22, 2708–2722.
- McAlpine, D., Jiang, D., and Palmer, A.R. (2001). A neural code for low-frequency sound localization in mammals. *Nat. Neurosci.* 4, 396–401.
- McCormick, D.A., and Pape, H.C. (1990). Properties of a hyperpolarization-activated cation current and its role in rhythmic oscillation in thalamic relay neurons. *J. Physiol.* 431, 291–318.
- Nambu, A., and Llinas, R. (1994). Electrophysiology of globus pallidus neurons in vitro. *J. Neurophysiol.* 72, 1127–1139.
- Nolan, M.F., Malleret, G., Dudman, J.T., Buhl, D.L., Santoro, B., Gibbs, E., Vronskaya, S., Buzsáki, G., Siegelbaum, S.A., Kandel, E.R., and Morozov, A. (2004). A behavioral role for dendritic integration: HCN1 channels constrain spatial memory and plasticity at inputs to distal dendrites of CA1 pyramidal neurons. *Cell* 119, 719–732.
- Nolan, M.F., Dudman, J.T., Dodson, P.D., and Santoro, B. (2007). HCN1 channels control resting and active integrative properties of stellate cells from layer II of the entorhinal cortex. *J. Neurosci.* 27, 12440–12451.
- Oertel, D., Shatadal, S., and Cao, X.J. (2008). In the ventral cochlear nucleus Kv1.1 and subunits of HCN1 are colocalized at surfaces of neurons that have low-voltage-activated and hyperpolarization-activated conductances. *Neuroscience* 154, 77–86.
- Person, A.L., and Perkel, D.J. (2005). Unitary IPSPs drive precise thalamic spiking in a circuit required for learning. *Neuron* 46, 129–140.
- Plack, C.J., and White, L.J. (2000). Perceived continuity and pitch perception. *J. Acoust. Soc. Am.* 108, 1162–1169.
- Pollak, G.D., Gittelman, J.X., Li, N., and Xie, R. (2011). Inhibitory projections from the ventral nucleus of the lateral lemniscus and superior paraolivary nucleus create directional selectivity of frequency modulations in the inferior colliculus: a comparison of bats with other mammals. *Hear. Res.* 273, 134–144.
- Rall, W., Burke, R.E., Holmes, W.R., Jack, J.J., Redman, S.J., and Segev, I. (1992). Matching dendritic neuron models to experimental data. *Physiol. Rev.* 72 (4, Suppl), S159–S186.
- Rudolph, M., and Destexhe, A. (2005). An extended analytic expression for the membrane potential distribution of conductance-based synaptic noise. *Neural Comput.* 17, 2301–2315.
- Saldaña, E., and Berrebi, A.S. (2000). Anisotropic organization of the rat superior paraolivary nucleus. *Anat. Embryol. (Berl.)* 202, 265–279.
- Saldaña, E., Aparicio, M.A., Fuentes-Santamaria, V., and Berrebi, A.S. (2009). Connections of the superior paraolivary nucleus of the rat: projections to the inferior colliculus. *Neuroscience* 163, 372–387.
- Schofield, B.R. (1995). Projections from the cochlear nucleus to the superior paraolivary nucleus in guinea pigs. *J. Comp. Neurol.* 360, 135–149.
- Scholl, B., Gao, X., and Wehr, M. (2010). Non-overlapping sets of synapses drive on responses and off responses in auditory cortex. *Neuron* 65, 412–421.
- Scott, L.L., Mathews, P.J., and Golding, N.L. (2005). Posthearing developmental refinement of temporal processing in principal neurons of the medial superior olive. *J. Neurosci.* 25, 7887–7895.
- Seifert, R., Scholten, A., Gauss, R., Mincheva, A., Lichter, P., and Kaupp, U.B. (1999). Molecular characterization of a slowly gating human hyperpolarization-activated channel predominantly expressed in thalamus, heart, and testis. *Proc. Natl. Acad. Sci. USA* 96, 9391–9396.
- Snell, K.B., and Frisina, D.R. (2000). Relationships among age-related differences in gap detection and word recognition. *J. Acoust. Soc. Am.* 107, 1615–1626.
- Soltesz, I., Lightowler, S., Leresche, N., Jassik-Gerschenfeld, D., Pollard, C.E., and Crunelli, V. (1991). Two inward currents and the transformation of low-frequency oscillations of rat and cat thalamocortical cells. *J. Physiol.* 441, 175–197.
- Sommer, I., Lingenhöhl, K., and Friauf, E. (1993). Principal cells of the rat medial nucleus of the trapezoid body: an intracellular in vivo study of their physiology and morphology. *Exp. Brain Res.* 95, 223–239.
- Steriade, M., McCormick, D.A., and Sejnowski, T.J. (1993). Thalamocortical oscillations in the sleeping and aroused brain. *Science* 262, 679–685.
- Wahl-Schott, C., and Biel, M. (2009). HCN channels: structure, cellular regulation and physiological function. *Cell. Mol. Life Sci.* 66, 470–494.
- Walton, J.P. (2010). Timing is everything: temporal processing deficits in the aged auditory brainstem. *Hear. Res.* 264, 63–69.

Wang, J., Chen, S., Nolan, M.F., and Siegelbaum, S.A. (2002). Activity-dependent regulation of HCN pacemaker channels by cyclic AMP: signaling through dynamic allosteric coupling. *Neuron* 36, 451–461.

Williams, S.R., and Mitchell, S.J. (2008). Direct measurement of somatic voltage clamp errors in central neurons. *Nat. Neurosci.* 11, 790–798.

Xie, R., Gittelman, J.X., and Pollak, G.D. (2007). Rethinking tuning: in vivo whole-cell recordings of the inferior colliculus in awake bats. *J. Neurosci.* 27, 9469–9481.

Zook, J.M., and Casseday, J.H. (1982). Cytoarchitecture of auditory system in lower brainstem of the mustache bat, *Pteronotus parnellii*. *J. Comp. Neurol.* 207, 1–13.